SAE TECHNICAL PAPER SERIES

2006-01-0038

Effects of Control Strategy and Calibration on Hybridization Level and Fuel Economy in Fuel Cell Hybrid Electric Vehicle

Kyung-Won Suh and Anna G. Stefanopoulou
University of Michigan, Ann Arbor

Reprinted From: Applications of Fuel Cells in Vehicles 2006 (SP-2006)

ISBN 0-7680-1720-3

2006 SAE World Congress
Detroit, Michigan
April 3-6, 2006

The Engineering Meetings Board has approved this paper for publication. It has successfully completed SAE's peer review process under the supervision of the session organizer. This process requires a minimum of three (3) reviews by industry experts.

ISSN 0148-7191

2006-01-0038

Effects of Control Strategy and Calibration on Hybridization Level and Fuel Economy in Fuel Cell Hybrid Electric Vehicle

Kyung-Won Suh and Anna G. Stefanopoulou
University of Michigan, Ann Arbor

ABSTRACT

Using dynamic causal models for a direct-hydrogen fuel cell and a DC/DC converter we design decentralized and multivariable controllers regulating the bus voltage and preventing fuel cell oxygen starvation. Various controller gains are used to span the fuel cell operation from load-following to load-leveling, and hence, determine the required fuel cell-battery sizing (hybridization level) and the associated trends in the fuel economy.

Our results provide insight on the strategy and calibration of a fuel cell hybrid electric vehicle with no need for a supervisory controller that typically depends on optimal power split during a specific driving cycle. The proposed controllers directly manipulate actuator commands, such as the DC/DC converter duty cycle, and achieve a desired power split. The controllers are demonstrated through simulation of a compact sedan using a mild and an aggressive driving cycle.

INTRODUCTION

The proton exchange membrane (PEM) fuel cell (FC) system for use in transportation needs to satisfy stringent requirements on transient performance and reliability. The overall system should function with a high degree of reliability under a wide range of conditions. Therefore the public success of fuel cell vehicles (FCV) depends on robust fuel cell operation based on system integration and control.

The control of a PEM fuel cell mainly consists of reactant supply, water/temperature, and power management. Lack of robustness on these control sub-systems can cause cross-coupled failures. The fuel cell, running with high reactant utilization, can often suffer from partial oxidant starvation in dynamic load changes even with optimized flow field design. Insufficient gas flow associated with dynamic load may cause accumulation of excess water, possibly blocking reactant diffusion. These anomalous operating conditions can cause not only reversible performance decrease but irreversible degradation [1].

Hybridization in various electric power configurations with the fuel cell stack, DC/DC converter and battery, such as the one shown in Figure 1, offers flexibility in managing the power demand from the fuel cell [2]. For instance, a load-following fuel cell supplies the majority of power to the load with a small energy buffer responsible for parasitic losses or start-up procedures [3]. In a load-leveling fuel cell hybrid system, the battery complements the fuel cell power during transient loading. Hybridization in the fuel cell power system may protect the fuel cell from harmful transition and in addition may achieve higher fuel cell efficiency by leveling peak power demand from the FC.

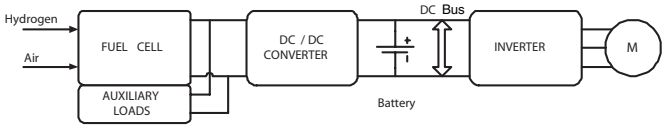

Figure 1: Fuel cell hybrid electric vehicle configuration

The efficiency of fuel cells is generally calculated by the produced electric energy as the output and heating value of hydrogen as the input [4]. The cell voltage also can be used as indication of the fuel cell efficiency. However, battery efficiency cannot be calculated directly because the losses in battery during charging-discharging are varying with current. Total vehicle level efficiency can be compared through the consumed hydrogen fuel during specific driving cycles.

The anticipated benefits of hybridization for fuel cell vehicle differ from those for internal combustion engine (ICE) vehicle. Hybridization in ICE vehicle enables the decoupling of the instantaneous torque and speed demands from the wheels, and in this way, it enforces the optimum engine operation. The fuel cell hybrid electric vehicle, on the other hand, has high efficiency at wide range of power levels so it is not clear if hybridization will increase efficiency in any significant manner to justify the increase in weight and complexity associated with the addition of the batteries. In both cases, regenerative braking helps capture and reuse the energy, improving fuel economy. Indeed [5] shows that a battery-hybrid fuel cell vehicle associated with regenerative braking improves efficiency up to 15 %. The efficiency gain in a fuel cell hybrid vehicle depends on the degree of hybridization [6]. The hybrid system efficiency can be worse than the stand-alone fuel cell in some driving cycles [3, 7].

These unexplored issues highlight the importance of defining the achievable performance of a fuel cell power system and then the minimum level of hybridization. Therefore we first establish a mathematical model of a PEM fuel cell stack with a compressor driven directly by the fuel cell power. The electrically connected FC and compressor allow us to design a realistic air delivery controller for regulating the oxygen excess ratio and to capture the FC performance limitation during abrupt changes in the current drawn (load) from the fuel cell. The dynamic coupling between the voltages and currents among the fuel cell, battery and the traction load is captured by a dynamic model of the DC/DC converter as shown in the electric hybrid configuration of Figure 1. A converter controller is then designed to boost and regulate the voltage at the converter output. Good regulation of the voltage at the converter output is typically achieved by large current drawn from the fuel cell and it is typically followed by small currents drawn from the battery. The converter controller can be tuned to avoid causing abrupt current draw from the fuel cell. In this paper, various DC/DC converter controller gains result in different levels of power split between the fuel cell and the battery. It is thus possible to assess the effects of control calibrations on the power split, FC oxygen excess ratio, compressor behavior, and vehicle efficiency.

Apart from exploring the effects of control calibration, we also clarify the benefits of coordination between the FC and the converter controller. In industry, due to proprietary concerns the DC/DC converter controller is traditionally treated separately from the fuel cell controller, similarly to what we are presenting in the first sections of this paper. In the last section, we introduce coordination between the DC/DC converter controller and the FC controller into a combined system controller with optimal gains that emulates an FC load-following power split scenario. The centralized control accounts for the limitations in the fuel cell system and allows us to construct a controller for the smallest possible power assist level without compromising the fuel cell operation. The results of fuel economy and battery sizing with the dynamic model and control in this work provide insight on the necessary hybridization of a fuel cell power system without employing cycle-dependent optimization.

FUEL CELL HYBRID VEHICLE MODEL

A complete PEM fuel cell propulsion power system includes several components apart from the fuel cell stack and battery, such as an air delivery system which supplies oxygen using a compressor or a blower, a hydrogen delivery system using pressurized gas storage or reformer, a thermal and water management system that handles temperature and humidity, DC/DC converters to condition the output voltage and/or current of the stack and finally inverter/traction motor [2]. Figure 1 shows the configuration of a typical fuel cell power system which is constructed with fuel cell, DC/DC converter and battery.

This paper presents details of the fuel cell system configuration and control that provides system analysis with transient response characteristics. A complete forward-facing, causal model for a fuel cell hybrid vehicle is desirable for component evaluation and detailed control simulation. The performance can be evaluated for each component and system in dynamic simulation of the forward-facing model. Interaction among the driver command, vehicle dynamics, traction motor load, power converters and power sources can be highlighted.

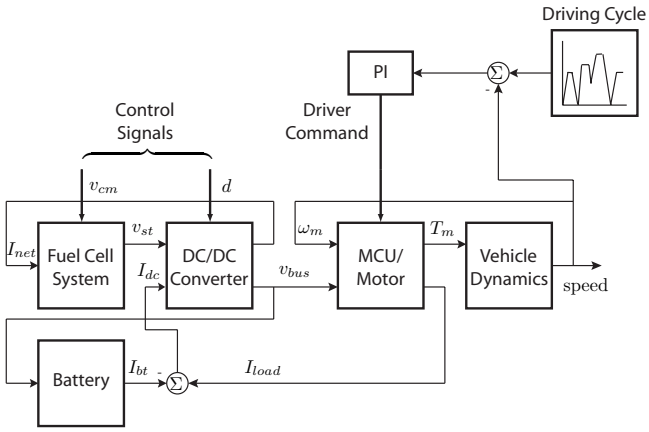

Figure 2: FC HEV powertrain causality flowchart

Figure 2 depicts the causal flow chart of a fuel cell hybrid vehicle model in Figure 1. The fuel cell hybrid vehicle model in this paper includes not only the forward-facing vehicle and traction motor model but also complete causal models for the fuel cell system, the DC/DC converter and the battery. The fuel cell system model includes reactant supply and flow-pressure relations with the input command of air compressor motor. The DC/DC converter is modeled with the duty cycle as the input. Therefore it is possible to design controllers and evaluate the feasibility of fuel cell sub-systems in terms of the dynamic performance and power losses.

Specifically, the air-supply sub-system and its dynamic control is implemented and evaluated. The model captures the dynamic effect of the air supply compressor, which results in major power losses in a direct hydrogen fuel cell system. In this model, regenerative braking is not included to concentrate on the interaction between the FC, battery and the load. The model for regenerative braking can be added to charge the battery by the current from the motor after isolating the fuel cell. Cold start and shutdown are not considered in this paper. For this study, the fuel cell hybrid vehicle characteristics are assumed to be based on a compact sedan. The values of the parameters are shown in Table 1.

Table 1: Baseline Vehicle Characteristics

Vehicle	
Total vehicle mass	1591 kg
Aerodynamic drag coefficient	0.312
Frontal area	2.06 m^2
Rolling resistance coefficient	0.02
Accessory load (WTM)	500 W
Fuel cell system	
Number of cells	381
Active area	280 cm^2
Maximum current	320 A
Temperature	80℃
Maximum power (stack)	75 kW
Maximum power (system)	60 kW
Compressor	Turbocompressor
Battery system	
Battery	Lead-acid
Capacity	18 Ah
Number of modules	31
Nominal voltage	400 V

MOTOR CONTROL UNIT/MOTOR, VEHICLE MODEL In an FC electric hybrid drive train, the driver control command directly manipulates the torque/power of the traction motor. In actual vehicle, the driver command is interpreted as a variable frequency/amplitute command through the DC/AC inverter and AC machine. In this paper, inverter, motor and control unit are modeled as static maps with the driver torque demand, the speed of the motor ω_m and the DC-bus voltage v_{bus} as inputs and the load current I_{load} as output. Therefore, the traction power is drawn from the fuel cell and the battery.

The motor torque T_m generated following the driver command forms the traction force of the vehicle. The vehicle speed is the output of first order vehicle dynamics associated with its mass and other parameters through the traction force. In driving cycle simulation, the driver command is the output from a proportional-integral (PI) controller that is designed for tracking the speed of a given cycle.

FUEL CELL SYSTEM MODEL The fuel cell system model in this paper captures dynamic performance in power including effects of parasitic losses. The model also predicts oxygen starvation from the dynamics of its air supply system. The performance variables for the FC power system are (i) the stack voltage v_{st} which directly influences the stack power $P_{fc} = v_{st}I_{st}$ when the current I_{st} is drawn from the stack, and (ii) the oxygen excess ratio λ_{O_2} in the cathode that indicates the level of oxygen supply to the stack. The FC system configuration is depicted in Figure 3.

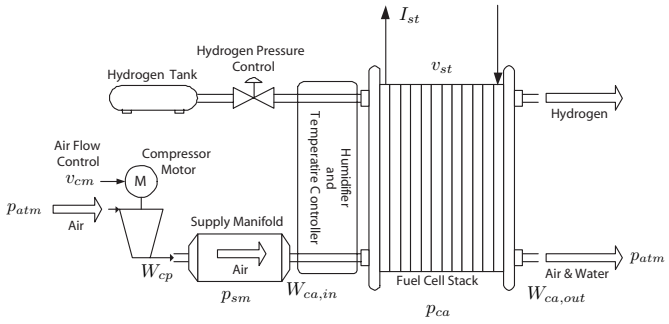

Figure 3: Fuel cell reactant supply system

Stack voltage is calculated as the product of the number of cells and average cell voltage $v_{st} = nv_{fc}$. The combined effect of thermodynamics, kinetics, and ohmic resistance determines the output average cell voltage

$$v_{fc} = E - v_{act} - v_{ohm} - v_{conc} \quad (1)$$

where E is the open circuit voltage, v_{act} is the activation loss, v_{ohm} is the ohmic loss, and v_{conc} is the concentration loss. The detailed equation of the FC voltage, also known as the polarization characteristic, can be found in [8].

The FC voltage has rich dynamic behavior due to its dependance on dynamically varying stack variables such as current density $i_{fc} = I_{st}/A_{fc}$, oxygen and hydrogen partial pressures p_{O_2} and p_{H_2}, and cathode pressure p_{ca}. Depending on the current drawn from the fuel cell and the air supply to the fuel cell, the stack voltage varies between 220 V and 350 V.

The total current drawn from the fuel cell stack, I_{st} is defined by the net current I_{net} which is the current from the FC to the DC/DC converter (in Figure 2), and augmented by the current load drawn from all of the auxiliaries and particularly from the compressor motor, I_{cm},

$$I_{st} = I_{net} + I_{cm}. \quad (2)$$

Here it is considered that the compressor motor contributes the largest percent of losses [9]. In this paper, the compressor power P_{cm}, or current I_{cm} is supplied directly from the fuel cell instead of a secondary battery, establishing a power-autonomous fuel cell system that provides net current I_{net}.

We assume a compressed hydrogen supply as shown in Figure 3, which simplifies the control of anode reactant flow. We also assume that the anode pressure is regulated to follow the cathode pressure. Controlled anode pressure can be achieved either with anode recirculation or a dead-ended anode outlet. The cooler and humidifier are neglected for this work because their power requirements are much smaller than that of the compressor [10].

The dynamic behavior of the variables associated with the air flow control, namely, oxygen pressure p_{O_2}, total cathode pressure p_{ca}, and oxygen excess ratio in the cathode λ_{O_2} can be found in [8]. The flow dynamics of the oxygen and hydrogen reactants are governed by pressure dynamics through flow channels, manifolds and orifices.

Mass continuity of the oxygen and nitrogen inside the cathode volume and the ideal gas law yield

$$\frac{dp_{O_2}}{dt} = \frac{\bar{R}T_{st}}{M_{O_2}V_{ca}}\left(W_{O_2,in} - W_{O_2,out} - W_{O_2,rct}\right), \quad (3)$$

$$\frac{dp_{N_2}}{dt} = \frac{\bar{R}T_{st}}{M_{N_2}V_{ca}}\left(W_{N_2,in} - W_{N_2,out}\right) \quad (4)$$

where V_{ca} is the lumped volume of cathode, $\bar{R}$ is the universal gas constant, and M_{O_2} and M_{N_2} are the molar mass of oxygen and nitrogen, respectively.

The compressor motor state is associated with the rotational dynamics of the motor through thermodynamic equations. A lumped rotational inertia is used to describe the compressor rotational speed ω_{cp}

$$\frac{d\omega_{cp}}{dt} = \frac{1}{J_{cp}}\left(\tau_{cm} - \tau_{cp}\right) \quad (5)$$

where τ_{cm} is the compressor motor torque defined through the supplied power in (8) and τ_{cp} is the load torque of the compressor calculated through nonlinear maps supplied by the manufacturer (function of pressure ratio, flow, and compressor speed).

The rate of change of air pressure in the supply manifold that connects the compressor with the fuel cell (shown in Figure 3) depends on the compressor flow into the supply manifold $W_{cp}(\omega_{cp}, p_{sm}, p_{atm})$, the flow out of the supply manifold into the cathode $W_{ca,in}$ and the compressor flow temperature T_{cp}

$$\frac{dp_{sm}}{dt} = \frac{\bar{R}T_{cp}}{M_{a,atm}V_{sm}}\left(W_{cp} - W_{ca,in}\right) \quad (6)$$

where V_{sm} is the supply manifold volume and $M_{a,atm}$ is the molar mass of atmospheric air.

The supply manifold model describes the mass flow rate from the compressor to the outlet mass flow. A linear flow-pressure condition $W_{ca,in} = k_{ca,in}(p_{sm} - p_{ca})$ is parameterized experimentally after assuming small pressure difference between the supply manifold pressure p_{sm} and the cathode pressure p_{ca} which is the sum of oxygen, nitrogen and vapor partial pressures $p_{ca} = p_{O_2} + p_{N_2} + p_{sat}$ where p_{sat} is the vapor saturation pressure. The total flow rate at the cathode exit $W_{ca,out}(p_{ca}, p_{atm})$ is calibrated with the nozzle flow equation because the pressure difference between the cathode and the ambient pressure is large in pressurized stacks.

The rate of oxygen consumption $W_{O_2,rct} = M_{O_2}\frac{nI_{st}}{4F}$ in (3) depends on the stack current I_{st} and the Faraday number F. The oxygen excess ratio

$$\lambda_{O_2} = \frac{W_{O_2,in}}{W_{O_2,rct}} \quad (7)$$

is typically regulated at $\lambda_{O_2}^{ref} = 2$ to reduce the formation of stagnant vapor and nitrogen films in the electrochemical reaction area. Values of λ_{O_2} lower than 1 indicate oxygen starvation and have serious consequences for stack life.

The compressor motor torque $\tau_{cm} = P_{cm}/\omega_{cp}$ depends on the power

$$P_{cm} = v_{cm}(v_{cm} - k_v\omega_{cp})/R_{cm} \quad (8)$$

provided by the compressor motor, which is calculated using the compressor motor voltage input v_{cm} and its rotational speed ω_{cp} assuming an ideal DC motor.

To calculate the current consumed by the compressor, we assume again that the compressor motor has an ideal power transformer and supplies the necessary power P_{cm} in (8) by drawing a current I_{cm} at the stack bus voltage v_{st},

$$I_{cm} = P_{cm}/v_{st} \quad (9)$$

where v_{st} is given by the polarization curve in [8]. Thus the compressor motor current, that adds to the current drawn by the DC/DC converter from the fuel cell, is implemented so that P_{cm} is simply drawn from the stack through a compressor motor control unit instantaneously.

DC/DC CONVERTER MODEL The DC/DC converter transforms the DC fuel cell stack power to the output voltage-current requirements of the external power devices that connect to the FC system. Here we consider a DC/DC converter (shown in Figure 4) boosting stack voltage to the 400 V DC-bus (v_{bus}).

The input voltage v_{st} and current I_{net} of the converter are the FC output voltage and the net FC current. The output voltage v_{bus} depends on the output current I_{dc} and the duty cycle d of the solid state switch in the circuit. The inductance of the input inductor L_{in} and the capacitance of the output capacitor C_{out} are shown in Figure 4.

An average nonlinear dynamic model can be used to approximate the boost converter switching dynamics

$$L_{in}\frac{dI_{net}}{dt} = v_{st} - (1-d)v_{bus},$$

$$C_{out}\frac{dv_{bus}}{dt} = (1-d)I_{net} - I_{dc} \quad (10)$$

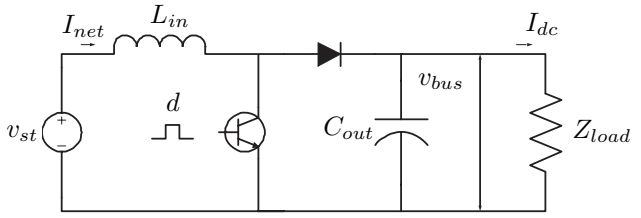

Figure 4: DC/DC boost converter

with inputs I_{dc} and v_{st} and outputs, the bus voltage v_{bus} and the current from the fuel cell I_{net}.

BATTERY MODEL The battery current is determined by an internal resistance model. The battery open circuit voltage v_o and the internal resistance R_{int} are static functions of the battery state of charge (SOC) as shown in Figure 5 (a) and temperature T. The internal resistance of the battery also changes with sign of the current, or charging/discharging as shown in Figure 5 (b). Assuming the battery is placed in parallel with the DC/DC converter, as shown in Figure 1, the terminal voltage of each battery module is determined by the DC-DC converter ($v_{bt} = v_{bus}/31$) and the battery current is then

$$I_{bt} = \frac{v_o(SOC, T) - v_{bt}}{R_{int}(SOC, sign(I_{bt}), T)}. \quad (11)$$

Here we assume that the battery temperature is maintained constant with an external cooling circuit. The battery parameters are based on ADVISOR model [11].

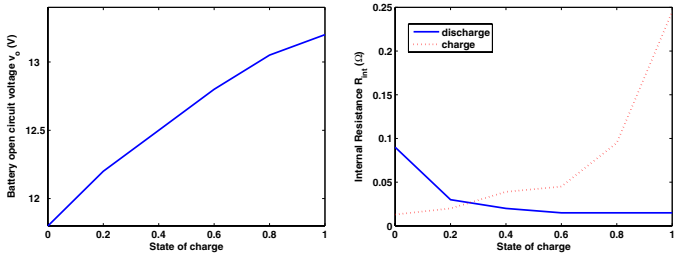

(a) Battery open circuit voltage v_o (b) Internal resistance R_{int}

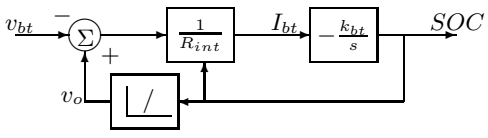

(c) Block diagram

Figure 5: Battery model

The SOC is calculated from the battery current and the capacity of the battery ($1/k_{bt}$)

$$\frac{dSOC}{dt} = -k_{bt} I_{bt}. \quad (12)$$

Figure 5 (c) shows the block diagram of the battery model and the relationship between the battery parameters, R_{int} and v_o, and the state of charge.

To insure proper shut down and start-up power from the battery, the battery should remain half charged. The SOC of each of the 31 battery modules is indeed maintained at 0.6 as shown later by regulating the bus voltage at 400 V. Note that at SOC=0.6 a battery module has open circuit voltage of 12.9 V (Figure 5 (a)), thus 31 modules at SOC=0.6 can be connected in parallel with the 400 V bus.

CONTROL OF FC HYBRID POWER

In most cases, the fuel cell with its compressor and compressor controller is viewed as one sub-system and the converter with its controller as another. Two different control objectives, oxygen excess ratio regulation in the fuel cell and bus voltage (or battery SOC) regulation in the DC/DC converter are pursued by two controllers. The two controllers are calibrated separately and small corrections are performed after the two sub-systems are connected. This control strategy is called decentralized and is traditionally followed in industry due to proprietary concerns between the FC and the DC/DC converter manufacturers. The calibration is called sequential, because one controller is tuned and then the other is re-tuned for a reasonable tradeoff between the two objectives.

CONTROL OF THE AIR SUPPLY SUB-SYSTEM In PEM fuel cells fed by compressed high-purity hydrogen, dynamic performance in the range of 0.1-1 second mainly depends on the air supply sub-system [9]. Excluding start-up and shut down periods, the transient response associated with controlling air and avoiding oxygen starvation is a key factor in hybrid vehicle design. To concentrate on control of the air supply, the humidity and temperature of the fuel cell stack is assumed to be controlled perfectly by dedicated hardware and controller.

The control objective of regulating the oxygen excess ratio λ_{O_2} can be achieved by a combination of feedback and feedforward algorithms that automatically defines the compressor motor voltage input v_{cm}. Since the oxygen excess ratio λ_{O_2} is not directly measured, we control λ_{O_2} indirectly by measuring the compressor air flow rate W_{cp} and the demanded load current I_{st}. Figure 6 shows the feedback and feedforward controllers which are designed to regulate the oxygen excess ratio in an autonomous fuel cell power system.

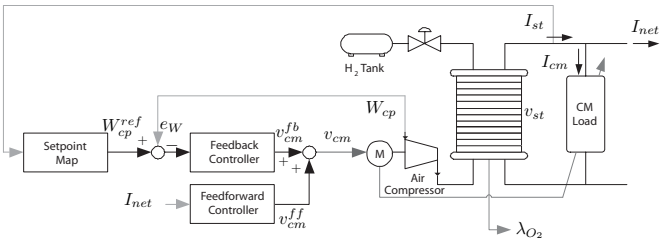

Figure 6: Schematic of fuel cell with air flow control using compressor

A feedforward controller is essential for oxygen excess ratio regulation because the compressor air flow is far from the cathode inlet and there is only an indirect measurement of λ_{O_2}. Feedforward control can accurately regulate λ_{O_2} to its desired value at steady-state if all the model parameters are known. Specifically, feedforward control to air compressor voltage v_{cm}^{ff} can be applied based on the net current to the load, I_{net}, i.e. the compressor motor voltage is $v_{cm}^{ff} = f(I_{net})$ [12].

To improve steady-state λ_{O_2} regulation despite modeling errors or device aging, the feedforward controller v_{cm}^{ff} can be combined with a feedback controller based on the compressor flow measurement W_{cp} (shown in Figure 6). The setpoint map in Figure 6 defines the demanded air flow rate W_{cp}^{ref} for the flow rate measurement position based on the stack current measurement [13], the desired oxygen excess ratio $\lambda_{O_2}^{ref}$ and the atmospheric humidity ratio w_{atm}

$$W_{cp}^{ref}(I_{st}, \lambda_{O_2}^{ref}) = (1 + w_{atm})\frac{1}{x_{O_2}}\lambda_{O_2}^{ref} M_{O_2}\frac{nI_{st}}{4F}. \quad (13)$$

A proportional and integral (PI) controller can be applied to the difference of W_{cp} and W_{cp}^{ref}. Finally the compressor control command can be written as

$$\begin{aligned} v_{cm}(t) &= v_{cm}^{ff}(t) + v_{cm}^{fb}(t) \\ &= f(I_{net}) + K_P\left(W_{cp}^{ref}(I_{st}(t)) - W_{cp}(t)\right) \\ &\quad + K_I\int_0^t \left(W_{cp}^{ref}(I_{st}(\tau)) - W_{cp}(\tau)\right) d\tau. \quad (14) \end{aligned}$$

Regulating air flow based on the flow rate measurement at the supply manifold inlet has a potential limitation because the actual air flow at the cathode inlet is not the same as that at the compressor outlet. The volume of supply manifold including humidifier and heat exchanger after the flow meter causes significant lag or delay on regulating oxygen excess ratio inside the stack [8, 14]. On the other hand, using a large compressor control effort may overcome the limitation above at the risk of causing instabilities when the compressor draws current directly from the stack [12, 15]. To address these limitations, the load current to the fuel cell stack should be shaped (filtered) to match the dynamic performance of the air sub-systems.

POWER CONVERTER CONTROL In the DC/DC converter model described in Figure 4 and (10), the only control input is the duty cycle of the DC/DC converter. The duty cycle, the actual control command to the DC/DC converter, is controlled in order to achieve the following objectives: (a) protect the fuel cell system from abnormal load including transient (b) maintain state of charge of the battery (c) maintain the DC-bus voltage v_{bus} (d) regulate the current (from both the fuel cell and battery) to the optimized values if supervisory control demand exists. A control strategy for splitting power between the fuel cell and the battery is implemented based on controlling the duty cycle of the DC/DC converter. In our case, the fuel cell is augmented with the DC/DC boost converter, matching the voltage of the DC-bus, v_{bus} to the desired value v_{bus}^{ref}. By changing the duty cycle, the net current of the fuel cell and the voltage of the battery which is equal to the bus voltage can be regulated, but not independently from each other.

Figure 7 shows the controller design for a DC/DC converter. Dual loop control (voltage/current control) can be implemented for the DC/DC boost converter [16]. Both current of the fuel cell, I_{net} and voltage of the bus, v_{bus} are controlled by the feedback controller. Regulating v_{bus} to a v_{bus}^{ref} is equivalent to regulating I_{bt} to zero due to the integration achieved naturally through the battery state of charge (see Figure 5). The regulation at zero battery current ensures that the battery serves as a power assist device without an explicit supervisory controller.

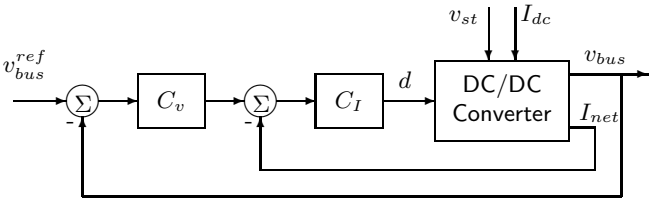

Figure 7: DC/DC boost converter control

In this control scheme, the outer loop controller C_v is composed of a proportional-integral (PI) controller for zero steady-state error in DC-bus voltage v_{bus}^{ref}. Then the output from C_v can be the virtual reference of I_{net}, which becomes the current drawn from the fuel cell when the converter connects to the fuel cell. A proportional controller (P) is used for the net fuel cell current controller C_I. Both P and PI controllers for C_v and C_I, respectively, can be tuned sequentially using classical control techniques. The C_v and C_I controllers can also be tuned using single-input, single-output classical proportional, integral and derivative (PID) control tuning techniques for regulating v_{bus}. Indeed, adding a proportional feedback C_I around the I_{net} measurement is equivalent to a derivative controller around v_{bus} which is needed to dampen the typically under-damped DC/DC converter dynamics [17].

We choose to apply a model-based linear quadratic regulator approach after transforming the C_v and C_I controllers to state feedback as follows. The controlled duty cycle d is

$$d(s) = -K_{Dv}I_{net}(s) - K_{Pv}v_{bus}(s) - \frac{K_{Iv}}{s}v_{bus}(s) \quad (15)$$

and formulated as state feedback when an integrator is added for the v_{bus} regulation objective. The optimal state feedback gains K_{Dv}, K_{Pv} and K_{Iv} can be selected from a linear quadratic regulator design. With known gains, the two equivalent controllers, C_v and C_I, are separated $C_v(s) = \frac{K_{Pv}}{K_{Dv}} + \frac{K_{Iv}}{K_{Dv}s}$ and $C_I(s) = K_{Dv}$.

If there is a pre-defined current command from the supervisory control or fuel cell system itself, the current loop (inner loop), C_I control can be used without the outer loop

C_v. The demanded current can be drawn from the fuel cell as fast as the control bandwidth of the inner loop allows. The supervisory command may decide the fuel cell current for optimal efficiency in terms of energy management or dynamic FC limitations such as oxygen starvation. Many FC manufacturers bundle their FC with a fuel cell controller unit that broadcasts the maximum FC current that is safe to draw from the FC. This signal can then be used with the inner loop controller C_I, eliminating the C_v controller. Nonlinear logic such as a slew rate limiter, saturation or filter can be added to shape the current demanded from the fuel cell stack. However, current control can lead to conservative operation of the fuel cell or excessive battery use. Due to the complexity and uncertainty in the fuel cell system, control of battery current has lower priority most times. Thus it is necessary to implement high fidelity logic that can handle the fuel cell and battery performance with extensive optimization.

The outer loop through the selection of C_v gains mainly handles the bus voltage regulation if there exists no supervisory control command. We define the DC/DC converter loop time constant τ_{DC} as the time needed to regulate v_{bus} within 63 % of v_{bus}^{ref} after a load disturbance I_{dc}. This time constant also defines how fast I_{net} is drawn from the FC and should be tuned to match the dynamic performance of the fuel cell system. The C_v calibration allows us to modify the fuel cell current request based on its impact on oxygen starvation or other dynamic limitations. The dual loop controller in (15) shows that the dual loop can manage the fuel cell system and battery performance in hybrid power and achieve different power split levels depending directly on the controller C_v gains and the achieved closed loop time constant τ_{DC}.

DISCUSSION OF SIMULATION RESULTS

The simulation results from the causal model for the fuel cell hybrid powertrain show the impact of different sub-system control designs on the hybrid design. Two different control calibration emulating load-following and load-leveling scenarios were designed to demonstrate the characteristic of the fuel cell operation. Both control strategies use decentralized control to show the effect of controller design on the performance of oxygen supply and power split. Simulation comparison is performed first using the FTP (Federal Test Procedure) driving cycle, which emulates an urban route as shown in Figure 8. Battery and FC sizes are fixed in the simulation analysis to concentrate on the effect of the control strategy (effect of C_v calibration).

Figure 9 shows the simulation results for a portion of the FTP driving cycle with two different power control calibrations. First a controller calibration, that results in a load-leveling FC hybrid, is considered which uses limited FC power and relies on transient power from the battery. The power split is achieved by the DC/DC converter control in (15) with low bandwidth (τ_{DC}=2 s) in the voltage loop. The other strategy shown is a load-following FC, which uses

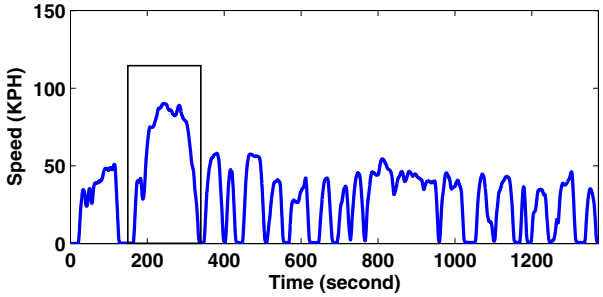

Figure 8: Vehicle speed on the FTP cycle

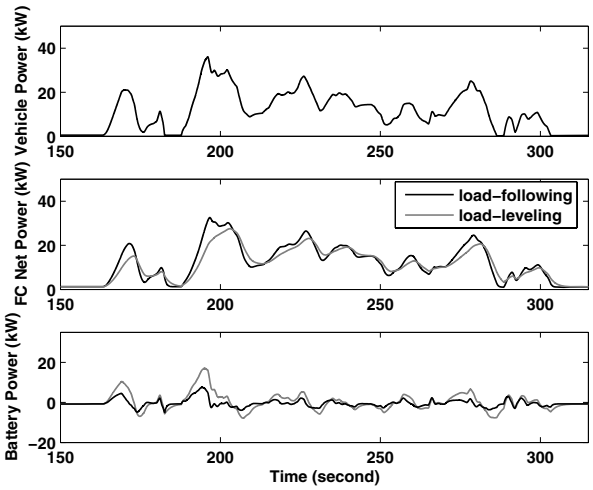

Figure 9: Power split in the FTP driving cycle with respect to control calibration

the FC power to the maximum whenever needed. The control calibration was performed by changing the bandwidth of the DC/DC converter response, i.e., fast response of the DC/DC converter for load-following FC operation (τ_{DC}=0.6 s).

During cycle simulation, the operating characteristics of the FC hybrid vehicle depend on the control calibration. Although both the load-leveling and load-following FC hybrid show limited FC net power below 36 kW, maximum power from the battery differs from 17 kW (load-leveling) to 7.5 kW (load-following). As can be seen in Figure 9, battery power is mostly used as transient power assist in load-leveling FC hybrid.

The changes in control calibration have limited effect on the fuel cell in the case of FTP driving cycle (mild power demand), leading to FC usage up to current density of 0.43–0.53 A/cm^2 as can be seen in Figure 10 (a) and (b). Even though load-following operation of FC shows higher power use in FC (0.53 A/cm^2), the histogram distribution (in the bar graph) shows similar overall characteristics. In both cases, the FC operates in the region of system efficiency over 45 %.

Simulation comparison is also performed on a portion of the US06 driving cycle which represents driving with hard-

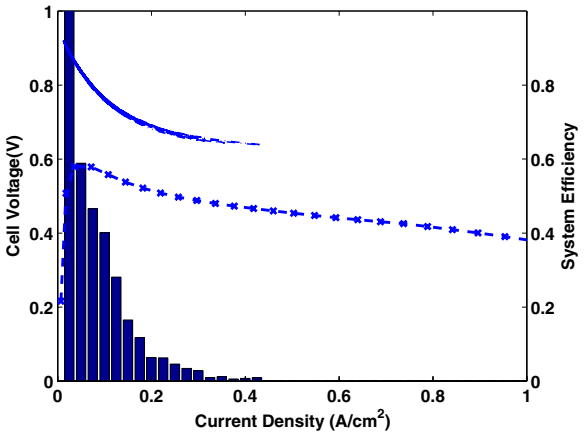

(a) Load-leveling FC

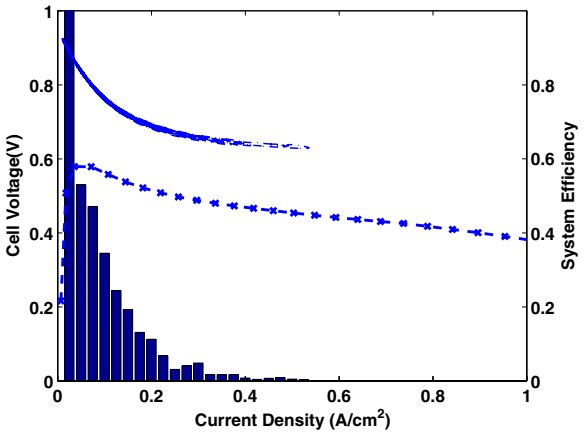

(b) Load-following FC

Figure 10: System efficiency (-x-), FC response ($\cdots$) and distribution (bar) for the FTP cycle

acceleration and high power demands as shown in Figure 11. Figure 12 shows the simulation comparison with two different power control calibrations during the portion of the US06 cycle. During aggressive demands in propulsion power, the operating characteristics of the FC depend on the control strategy. The load-leveling FC hybrid shows limited FC power up to 40 kW and uses battery power up to 30 kW. The load-following FC tuning uses FC power to satisfy approximately the maximum transient vehicle power demand of 50 kW.

In both cases, accurate air-supply and power-assist ensure regulation of oxygen supply in safe regimes as can

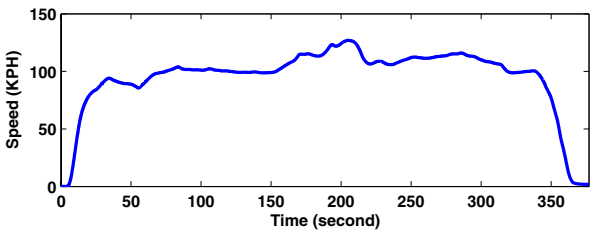

Figure 11: Vehicle speed on a portion of the US06 cycle

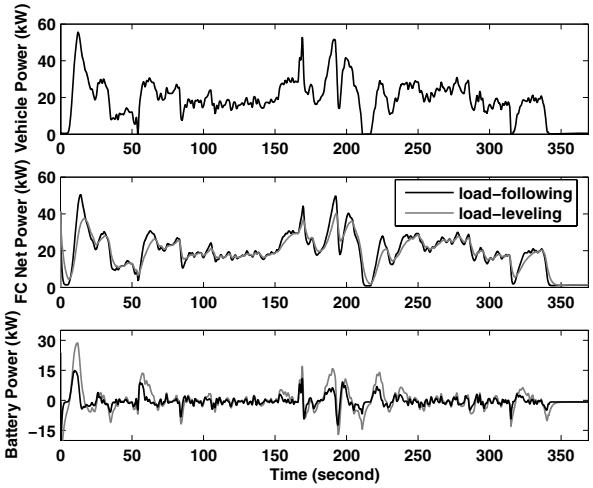

Figure 12: Power split in a portion of US06 driving cycle with respect to control calibration

be seen in Figure 13 (a) and Figure 14 (a). The oxygen excess ratio λ_{O_2} is well regulated around the desired setpoint ($\lambda_{O_2}^{ref} = 2$) without large excursion, which could cause oxygen starvation. The regulation is achieved despite the large currents drawn from the fuel cell, 0.7 A/cm^2 and 1 A/cm^2 for the load-leveling and load-following calibrations as shown in Figure 13 (b) and Figure 14 (b). As the power demand of the traction motor changes, deficit power from fuel cell is naturally covered by the battery for a short while. Battery current is not used when power from the fuel cell follows the motor load. The changes in SOC of the load-leveling system are larger than that of load-following system, but battery usage for power-assist is minimal in both cases as intended.

It is observed that the hydrogen fuel economy is almost invariant to the control tuning, being 66–67 MPGE (miles per gallon equivalent to the energy stored in one gallon of gasoline) on the FTP cycle and 44 MPGE on the US06 cycle as can be seen in Figure 15. As it is shown in Figures 10, 13 (b) and 14 (b), aggressive fuel cell use, which might lower the fuel cell efficiency during a load-following FC calibration, is only effective for a short period. Thus the hydrogen fuel consumption shows no difference overall with respect to control calibrations. However, the results in battery usage ΔSOC (0.51 % in load-following vs. up to 5 % in load-leveling for US06) and maximum power (15 vs. 30 kW) suggest that it is feasible to accommodate a smaller size battery, saving weight and volume in load-following FC. Thus, FC transient power response and not efficiency is the key consideration in sizing the battery in a hybrid FC vehicle.

As can be seen in λ_{O_2} and the battery current profile in Figure 14, minimizing battery power with load-following calibration is followed by larger deviation in oxygen excess ratio than that with load-leveling calibration. High bandwidth in regulating v_{bus} to v_{bus}^{ref} results in abrupt I_{net} variation and thus drop in λ_{O_2}. It is more clear in Figure 16

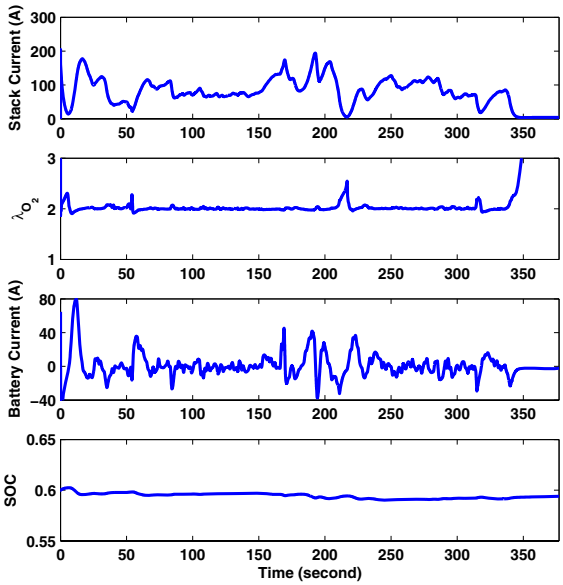

(a) FC current, oxygen excess ratio, battery current and SOC

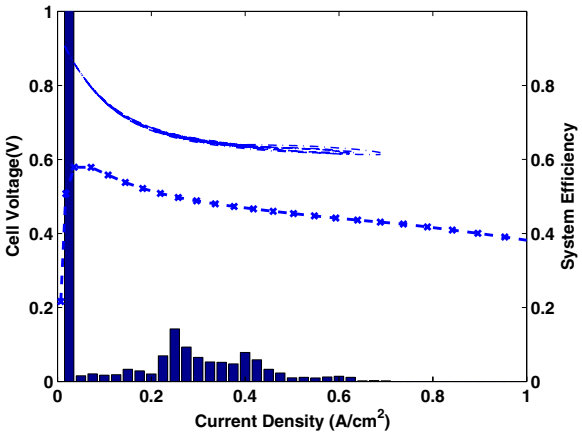

(b) System efficiency (-x-), FC response (···) and distribution (bar)

Figure 13: Fuel cell and battery operating characteristics of hybrid vehicles for a portion of the US06 cycle - load-leveling FC

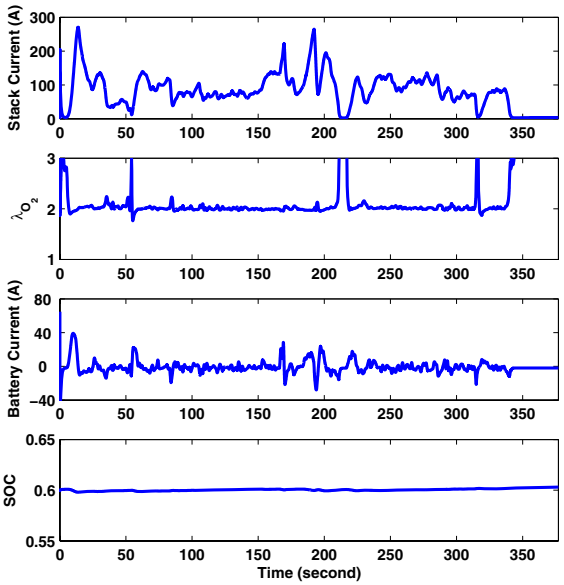

(a) FC current, oxygen excess ratio, battery current and SOC

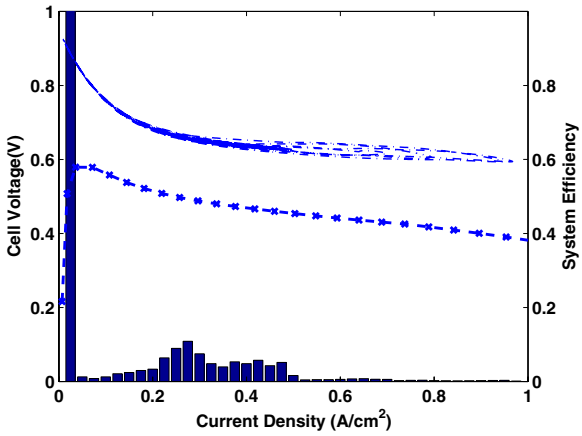

(b) System efficiency (-x-), FC response (···) and distribution (bar)

Figure 14: Fuel cell and battery operating characteristics of hybrid vehicles for a portion of the US06 cycle - load-following FC

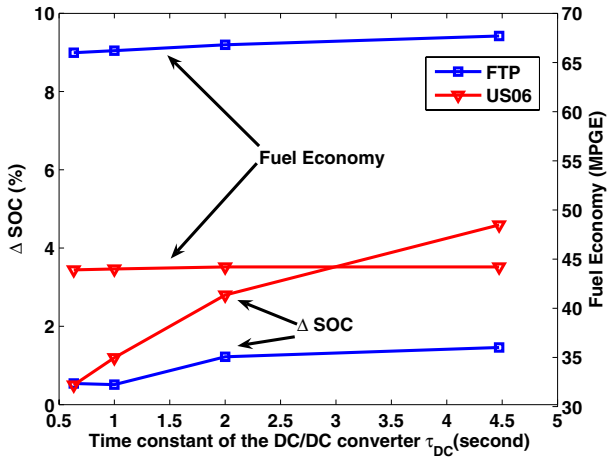

Figure 15: Battery usage and fuel economy with respect to controller calibration and the cycle

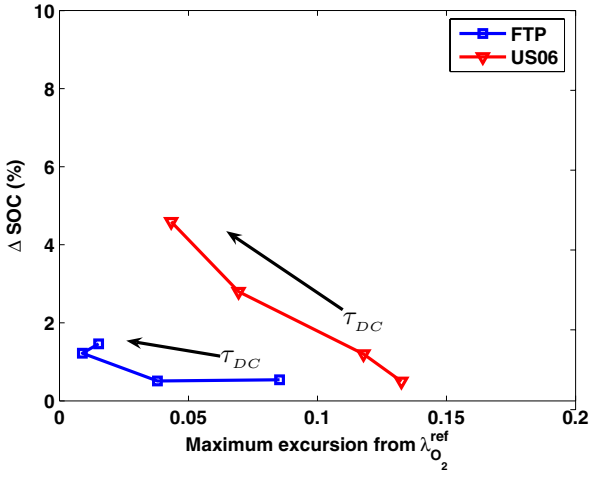

Figure 16: Battery usage and oxygen excess ratio with respect to controller calibration and the cycle

that there is a tradeoff between the two performance variables, namely, the battery SOC and oxygen excess ratio. The oxygen excess ratio regulation degrades when the SOC variations are reduced. Therefore, decision in controller tuning and battery sizing should be done under the specification for maximum allowable oxygen excess ratio deviation.

In the controller tuning, actuator limits should be also be taken into account. Specifically, in a high-pressure FC system with an air supply compressor, the dynamic behavior of the compressor imposes additional limitations through its surge and choke characteristics. Surge causes large variations in flow and choke is an upper limit to the compressor air flow. In a fuel cell system there is a potential for both compressor surge and choke during an abrupt decrease and increase, respectively, in the applied compressor voltage command v_{cm}. Figure 17 shows the compressor transient response with load-following FC on a portion of the US06 cycle. As can be seen in the Figure 17, the transient responses are mostly within the region of safe compressor operation, not falling into the surge region (left solid line) or choke region (right solid line). A more sophisticated control for surge prevention by manipulating current load can be found in [18].

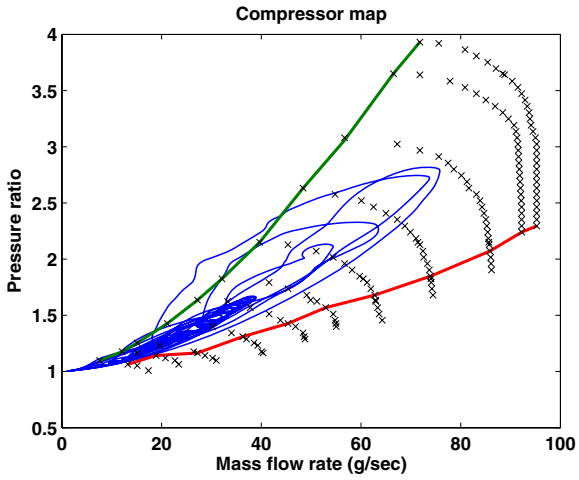

Figure 17: Compressor transient response(blue line) on static compressor map(x) with load-following FC power

Another significant compressor consideration arises from its parasitic loss and its effects on the FC system efficiency at low loads. Lowering the minimum air flow rate in the compressor helps in achieving high efficiency in low power ranges [19]. The minimum air flow rate in the compressor can be as low as 5 g/s (the air flow at the maximum power is 95 g/s) with the controller described in this paper. Also note here that the fuel cell model in this work is not turned off anytime during simulation because 500 W of accessary load is always applied independently of the vehicle speed. The simulation result shows that the FC efficiency is always over 40 % mainly because of low minimum air flow rate explained above (see all histograms of driving cycle simulations).

CENTRALIZED CONTROL

In fuel cell hybrid power systems, the performance variables, oxygen excess ratio and battery SOC, are defined through the interaction between the fuel cell system and DC/DC converter. Controller bandwidth of the DC/DC converter mainly determines SOC by v_{bus} regulation and λ_{O_2} through controlling current from the FC, I_{net}. Another control design that takes into account directly the tradeoff between small excursions in λ_{O_2} and SOC is called multivariable control and it results in a centralized controller as shown in Figure 18.

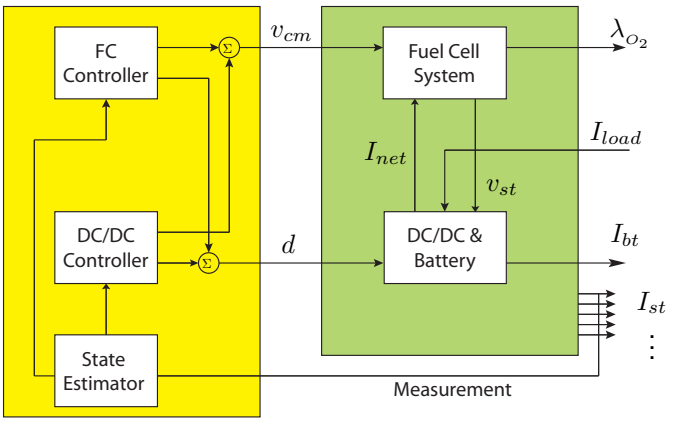

Figure 18: Centralized control architecture in fuel cell hybrid vehicle

We apply a model-based linear quadratic regulator approach for the whole FC-DC/DC-battery hybrid system. This coordinated control preserves the control authority on oxygen regulation and power distribution in the same way as decentralized control, and in addition introduces interaction between the FC and the converter controllers. The bandwidths achieved in the two decentralized controllers (v_{cm}-W_{cp} and d-v_{bus} loops) are preserved with the centralized controller. The resulting optimal control produces additional command to d through the estimated deviation in λ_{O_2}. Moreover, the v_{cm} command is now shaped through its effects to current drawn from the battery I_{bt}.

Note here that the centralized controller penalizes deviations of the battery current I_{bt} instead of v_{bus} in order to minimize SOC deviation. As can be seen from the decentralized load-following FC hybrid scheme (in Figure 14), reduced I_{bt} helps minimizing SOC indirectly. The information that is required for the centralized controller is collected by the state estimator designed from the various existing measurements, namely, the stack current I_{st}, the stack voltage v_{st} and the supply manifold pressure p_{sm} [17].

This communication and coordination help obtain accurate control in air delivery and improve transient FC performance. Communication between the FC controller and DC/DC controller yield optimized performance in coordinated control, resulting in minimal battery usage. Fig-

ure 19 shows the simulation result of the centralized control for the portion of the US06 cycle. As can be seen in the figure, the maximum current from the battery is limited to 30 A (or 12 kW power), compared with the 15 kW maximum power obtained from the load-following decentralized control in Figure 14. The variation in SOC is 0.39 %, which is lower than the 0.51 % achieved through the load-following decentralized control in Figure 15.

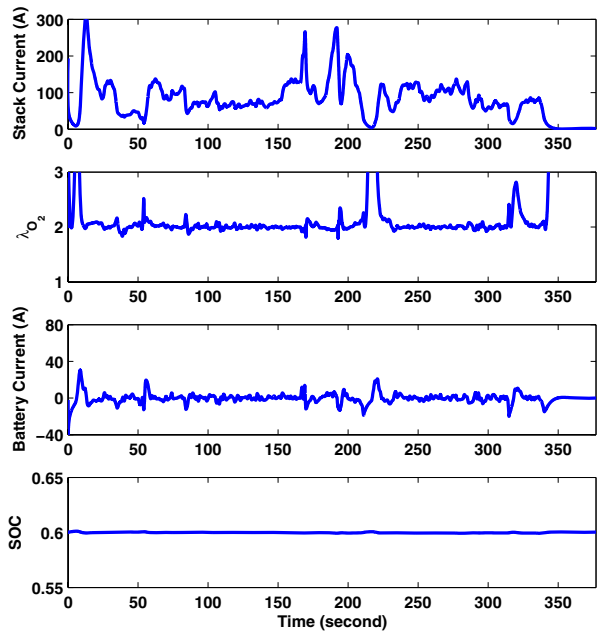

Figure 19: Fuel cell and battery operating characteristics of hybrid vehicles for a portion of the US06 cycle - centralized control

CONCLUSION

In this paper we consider a compact sedan fuel cell electric hybrid with a compressor driven 75 kW proton exchange membrane fuel cell, a boost DC/DC converter and a battery, and assess the effect of different control calibrations and strategies in the power split, the vehicle efficiency, the battery utilization and the FC oxygen starvation. A forward-facing (causal) model is used and the assessment is performed for two different driving cycles with mild (FTP) and aggressive (US06) accelerations.

The overall controller automates two processes. First, it adjusts the FC air flow through a compressor motor command to minimize oxygen starvation periods. Second, it regulates the bus voltage through the duty cycle of the boost converter. The FC compressor controller is novel because its calibration balances the benefits from the instantaneous flow increase and its drawbacks from the increase in the FC load (parasitic losses). Once the FC controller is tuned, a DC/DC converter controller is designed to transform the unregulated FC voltage to regulated bus voltage.

Different gains in the converter controller achieve different transient responses in the bus voltage regulation. Fast voltage regulation corresponds to a load-following FC calibration with high FC utilization and low battery utilization (50 kW in FC power versus 15 kW in battery power for the aggressive cycle). Slow voltage regulation results in a load-leveling FC calibration that does not exhibit any significant benefits when compared to the load-following calibration. The control calibration has minimal effect on fuel economy primarily because typical driving cycles can be accomplished by a well controlled FC with efficiencies up to 45 %. A smaller battery size (15 kW versus 30 kW) can reduce the vehicle weight and volume without adversely affecting the FC performance (efficiency, oxygen excess ratio) or requiring operation close to the compressor surge and choke limits.

The control design in this work deals with actual current and voltage instead of power unlike many other papers, respecting their causal relationship. Also the designed control system does not require inner loop controllers that realize the power split command from a supervisory controller since the designed controllers manipulate directly physical actuators setting in the FC stack system and the DC/DC converter. Therefore applying and re-tuning our control methodology to various hardware configurations can be done directly without cycle dependent optimization.

ACKNOWLEDGMENTS

This work is funded by NSF 0201332 and the Automotive Research Center (ARC) under U.S. Army contract DAAE07-98-3-0022.

REFERENCES

[1] S. D. Knights, K. M. Colbow, J. St-Pierre, and D. P. Wilkinson, “Aging mechanisms and lifetime of PEFC and DMFC,” *Journal of Power Sources*, vol. 127, pp. 127–134, 2004.

[2] K. Rajashekara, “Propulsion system strategies for fuel cell vehicles,” SAE paper 2000-01-0369, 2000.

[3] D. J. Friedman, “Maximizing direct-hydrogen PEM fuel cell vehicle efficiency - is hybridization necessary?” SAE paper 1999-01-0530, 1999.

[4] J. Larminie and A. Dicks, *Fuel Cell Systems Explained*, 2nd ed. Chichester and Hoboken, NJ: John Wiley & Sons, 2003.

[5] J. M. Cunningham, R. Moore, S. Ramaswamy, and K. Hauer, “A comparison of energy use for a direct-hydrogen hybrid versus a direct-hydrogen load-following fuel cell vehicle,” SAE paper 2003-01-0416, 2003.

[6] T. Ishikawa, S. Hamaguchi, T. Shimizu, T. Yano, S. Sasaki, K. Kato, M. Ando, and H. Yoshida, “De-

velopment of next generation fuel-cell hybrid system - consideration of high voltage system," SAE paper 2004-01-1304, 2004.

[7] S. Ramaswamy, R. Moore, J. M. Cunningham, and K.-H. Hauer, "A comparison of energy use for a indirect-hydrocarbon hybrid versus an indirect-hydrocarbon load-following fuel cell vehicle," SAE paper 2004-01-1476, 2004.

[8] J. T. Pukrushpan, H. Peng, and A. G. Stefanopoulou, "Control-oriented modeling and analysis for automotive fuel cell systems," *ASME Journal of Dynamic Systems, Measurement, and Control*, vol. 126, no. 1, pp. 14–25, 2004.

[9] J. M. Cunningham, M. A. Hoffman, R. M. Moore, and D. J. Friedman, "Requirements for a flexible and realistic air supply model for incorporation into a fuel cell vehicle (FCV) system simulation," SAE paper 1999-01-2912, 1999.

[10] D. D. Boettner, G. Paganelli, Y. G. Guezennec, G. Rizzoni, and M. J. Moran, "Proton exchange membrane fuel cell system model for automotive vehicle simulation and control," *ASME Journal of Energy Resources Technology*, vol. 124, pp. 20–27, 2002.

[11] V. H. Johnson, "Battery performance models in ADVISOR," *Journal of Power Sources*, vol. 110, pp. 321–329, 2002.

[12] W. E. Mufford and D. G. Strasky, "Power control system for a fuel cell powered vehicle," U.S. Patent 5 991 670, Nov. 23, 1999.

[13] G. Boehm, D. P. Wilkinson, S. Knights, R. Schamm, and N. J. Fletcher, "Method and appratus for operating a fuel cell," U.S. Patent 6 461 751, Oct. 8, 2002.

[14] P. Rodatz, G. Paganelli, and L. Guzzella, "Optimizing air supply control of a PEM fuel cell system," in *Proceedings of the 2003 American Control Conference*, vol. 3, Denver, CO, June 2003, pp. 2043–2048.

[15] K.-W. Suh and A. G. Stefanopoulou, "Inherent performance limitations of power-autonomous fuel cell system," in *IEEE Proceedings of 2006 American Control Conference, Submitted*.

[16] P. T. Krein, *Elements of Power Electronics*. New York and Oxford: Oxford University Press, 1998.

[17] K.-W. Suh and A. G. Stefanopoulou, "Coordination of converter and fuel cell controllers," *International Journal of Energy Research*, vol. 29, no. 12, pp. 1167–1189, 2005.

[18] A. Vahidi, I. Kolmanovsky, and A. G. Stefanopoulou, "Constraint management in fuel cells: A fast reference governor approach," in *IEEE Proceedings of 2005 American Control Conference*, Portland, OR, June 2005, pp. 3865–3870.

[19] P. Rodatz, G. Paganelli, A. Sciarretta, and L. Guzzella, "Optimal power management of an experimental fuel cell/supercapacitor-powered hybrid vehicle," *Control Engineering Practice*, vol. 13, no. 1, pp. 41–53, Jan. 2005.